

Multi-level Multiple Instance Learning with Transformer for Whole Slide Image Classification

Ruijie Zhang¹ Qiaozhe Zhang¹ Yingzhuang Liu¹ Hao Xin²
Yan Liu² Xinggang Wang^{1*}

¹Huazhong University of Science and Technology ²Ant Group
{klseki, qiaozhezhang, xgwang}@hust.edu.cn

Abstract

Whole slide image (WSI) refers to a type of high-resolution scanned tissue image, which is extensively employed in computer-assisted diagnosis (CAD). The extremely high resolution and limited availability of region-level annotations make employing deep learning methods for WSI-based digital diagnosis challenging. Recently integrating multiple instance learning (MIL) and Transformer for WSI analysis shows very promising results. However, designing effective Transformers for this weakly-supervised high-resolution image analysis is an underexplored yet important problem. In this paper, we propose a Multi-level MIL (MMIL) scheme by introducing a hierarchical structure to MIL, which enables efficient handling of MIL tasks involving a large number of instances. Based on MMIL, we instantiated MMIL-Transformer, an efficient Transformer model with windowed exact self-attention for large-scale MIL tasks. To validate its effectiveness, we conducted a set of experiments on WSI classification tasks, where MMIL-Transformer demonstrate superior performance compared to existing state-of-the-art methods, i.e., 96.80% test AUC and 97.67% test accuracy on the CAMELYON16 dataset, 99.04% test AUC and 94.37% test accuracy on the TCGA-NSCLC dataset, respectively. All code and pre-trained models are available at: <https://github.com/hustvl/MMIL-Transformer>

Introduction

Deep learning’s success (Hu et al. 2019; Huang et al. 2019; Ramachandran et al.; Wang et al. 2018a; Zhao, Jia, and Koltun 2020; Tan and Le 2019) in sequential image tasks offers promising methods for digital pathology. Whole slide images (WSIs), which are high-resolution digital slides of tissue specimens, are commonly used in image-based digital pathology (He et al. 2012). However, the huge size and absence of pixel/region-level annotations (Srinidhi, Ciga, and Martel 2021) in WSIs create obstacles for deep learning-based image diagnosis. To address the aforementioned problem, image-based computer-assisted diagnostics typically employ multiple instance learning (MIL) (Keeler, Rumelhart, and Leow 1990; Dietterich, Lathrop, and Lozano-Pérez 1997), a subset of weakly supervised learning methods (Zhou 2018).

*Xinggang Wang is the corresponding author
Copyright © 2024, Association for the Advancement of Artificial Intelligence (www.aaai.org). All rights reserved.

The dataset of a MIL task is organized into multiple bags, with each bag consisting of multiple instances. The annotations are only available at the bag level. This data organization offers significant benefits in the field of image-based digital pathology. For instance, in cancer diagnosis, the entire WSI (bag-level data) can be labeled as tumor without the necessity of distinguishing normal tissue (instances) within the WSI. This approach substantially alleviates the challenges associated with data and annotations acquisition. However, challenges persist due to the high resolution of WSI and the unbalanced distribution of instance categories.

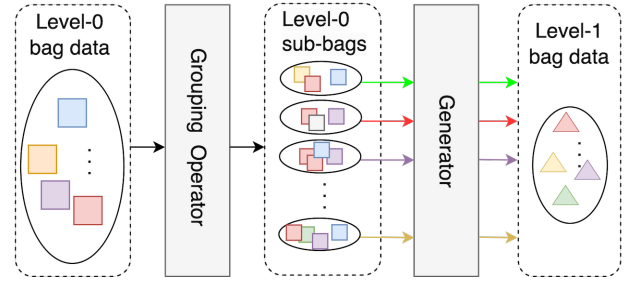


Figure 1: A two-level Multiple Instance Learning framework. 1) A bag is divided into several sub-bags by a grouping operator; 2) Perform multi-head self-attention (MSA) within sub-bags; 3) Making use of sub-bags in 2) to build higher-level bag data; 4) Hierarchical bags can be generated by repeating 1), 2) and 3).

Previous studies have explored the applications of MIL in digital pathology tasks. (Wang et al. 2018b; Kanavati et al. 2020) perform pooling operation on instance feature embeddings then to following tasks. (Ilse, Tomczak, and Welling 2018) introduce the attention mechanism, where trainable attention weights are given to each instance for aggregation. Li et al. (Li, Li, and Eliceiri 2021) introduced non-local attention to MIL, where the similarity is measured between the instance to give distinct attention weights. To introduce correlated information between instances, (Shao et al. 2021) uses Nyström Attention (Xiong et al. 2021) based transformer to calculate global attention between all instances in one bag.

Transformer (Vaswani et al. 2017) adopts the self-attention mechanism, which calculates the pairwise corre-

lation between each token within a sequence. Self-attention mechanism enables Transformer to effectively capture both the spatial morphology features of individual patches, as well as the correlation information between different patches (Chen et al. 2021). However, when working with high-resolution WSIs, Transformer would yield a prohibitively large number of patches, making it challenging to use the original self-attention mechanism. To address this problem, one approach is to use approximate attention (Xiong et al. 2021; Beltagy, Peters, and Cohan 2020), but may not capture all the intricate relationships within the sequence compared to the original self-attention mechanism. Another approach is to perform local-attention (Jaderberg et al. 2015; Liu et al. 2021), which can be classified into two strategies. The first strategy is a non-overlapped approach, reducing computational complexity to a great extent but lacking the capability to capture global information. The second strategy is overlapped approach, which enhances communication among local elements. Nonetheless, as the sequence length grows, this strategy introduces supplementary computational complexity (Fang et al. 2022).

In response to the aforementioned challenges, we propose the Multi-level MIL (MMIL), aiming at enabling non-approximate self-attention as well as building accurate local-to-global self-attention for large-scale multi-instance learning, i.e., the size of input instances can be up to more than 50k. Based on this strategy, we instantiated MMIL-Transformer for WSIs classification. We conducted a set of experiments on two public datasets, i.e., CAMELYON16 (Bejnordi et al. 2017) and TCGA-NSCLC (Tomczak, Czerwińska, and Wiznerowicz 2015) to demonstrate its effectiveness. The proposed model achieved a promising test AUC 96.80% and test accuracy 97.67% on the CAMELYON16 dataset, test AUC 99.04% and test accuracy 94.37% on the TCGA-NSCLC dataset. We expect our efforts can further ease the research and application of Transformers for large-scale MIL. We summarize our contributions as follows:

- We propose a differentiable multi-level MIL (MMIL) formulation, in which original instances can be flexibly grouped into sub-bags and each sub-bag will generate a new instance for final bag classification. Besides, various instance grouping methods, like *MSA grouping*, are proposed and studied.
- We propose MMIL-Transformer to conquer the high-resolution WSI classification problem, in which exact self-attention can be computed within local regions and the global WSI representation can be learned effectively. In addition, we design a masking mechanism by removing original instances to further boost performance and reduce computational costs.
- The proposed MMIL Transformer can obtain state-of-the-art WSI classification results on the challenging CAMELYON16 and TCGA-NSCLC datasets using both ResNet and ViT as patch encoders.

Related Work

Whole Slide Images Pre-processing

WSI scanners are capable of converting biopsy slide tissue into a gigapixel image by capturing the image in small, overlapping sections and stitching them together to form a high-resolution image of the entire slide, typically at $20\times$ to $40\times$ magnification. These images fully preserve the original tissue structure, which is crucial for computer-assisted diagnostics (CAD) (He et al. 2012). To read or manipulate WSI, there are several open-source tools available, such as OpenSlides (Goode et al. 2013) and QuPath (Bankhead et al. 2017). However, due to the presence of a large number of background images and noise images in WSI, it is necessary to perform corresponding processes on them. There are two main categories of methods for WSI processing. The first one is a classic image processing method, where the clipped WSI patches are converted to the HSV color space, and then subjected to background removal and denoising based on hue, Saturation and value (Tian et al. 2019). The second category is a deep learning based method (Lu et al. 2021; Li, Li, and Eliceiri 2021), where a classifier like CNN is trained to distinguish whether the clipped patches are tissue or not.

Multiple Instance Learning in Pathology

In the pathology field, MIL methods can be categorized into two types, instance-based MIL (Kanavati et al. 2020; Campanella et al. 2019; Xu et al. 2019; Lerousseau et al. 2020; Chikontwe et al. 2020) and embedding-based MIL (Lu et al. 2021; Shao et al. 2021; Li, Li, and Eliceiri 2021), based on the input data for aggregation module. Instance-based MIL methods first map extracted patches to pseudo-labels that correspond to the bag-level annotation, and then use these corresponding top-k instances for aggregation. Due to the unbalanced distribution of different instance types, instance-based methods always require a large number of WSIs. Embedding-based MIL methods first map extracted patches to embeddings then fed all patch feature embeddings to the following modules. Recently, attention mechanism have gained interest in MIL. (Ilse, Tomczak, and Welling 2018; Tomita et al. 2019; Hashimoto et al. 2020; Naik et al. 2020; Lu et al. 2021) introduce trainable weights to each instance. To further improve the performance, non-local attention (Li, Li, and Eliceiri 2021) and self-attention (Shao et al. 2021) is also adopted in MIL. Most previous MIL methods focused on evaluating the labels of instances, (Wang et al. 2018b) emphasizes the representation of bags. DGMIL (Qu et al. 2022) considers the feature distribution of WSIs and uses this information to guide MIL. DTFD-MIL (Zhang et al. 2022) introduces the concept of pseudo-bags to enlarge the number of bags. (Lin et al. 2023) addresses MIL from a novel perspective via analyzing the confounders between bags and labels.

Self-attention Mechanism

The inception of Transformer (Vaswani et al. 2017) can be traced back to the domain of natural language processing (NLP), where the self-attention mechanism plays a pivotal role in establishing relations between local features.

For gigapixel images, the patch sequence becomes too long to process in self-attention mechanism. Local-attention and approximate-attention can be employed to address this problem. (Beltagy, Peters, and Cohan 2020) introduce a fixed-size sliding window to sequences, MSA is only performed within the windows. (Child et al. 2019) propose sparse-Transformer, where a subset of the input sequence is selected by adaptive mechanisms to calculate self-attention. (Wang et al. 2020) introduce a low-rank factorization of the attention matrix. There are also other local-attention methods (Kitaev, Kaiser, and Levskaya 2020; Zaheer et al. 2020). However, local-attention methods present a trade-off dilemma where non-overlapped windows lack communication between each window, while overlapped windows make more computational burden as the sequence goes longer. And the adoption of approximate attention in models results in information loss, reducing the interpretability of the model. Therefore, we require a more efficient, simple, and flexible approach to building local-global relations to handle high-resolution images like WSIs. (Fang et al. 2022) proposed a messenger mechanism to the non-overlapped window attention method, which enables the information exchange between separated windows.

In MMIL-Transformer, we incorporate *MSG* mechanism (Fang et al. 2022) into MMIL as one method to establish a hierarchical framework. However, We do not treat *MSG* tokens only as a hub for communication between fixed windows. We use those tokens to generate higher-level instances, which finally contribute to higher-level bags. Moreover, we introduce an embedding-wise masking mechanism to further reduce the number of instances and boost the performance.

Method

Transformer-based Multiple Instance Learning

MIL Problem Formulation In MIL, given N bag-level samples $\{\mathbf{X}_1, \mathbf{X}_2, \dots, \mathbf{X}_N\}$ and their corresponding bag-level label $\{\mathbf{Y}_1, \mathbf{Y}_2, \dots, \mathbf{Y}_N\}$, each bag-level data \mathbf{X}_i is made of numbers of instances $\{\mathbf{x}_{i,1}, \mathbf{x}_{i,2}, \dots, \mathbf{x}_{i,n_i}\}$, where the instance-level labels $\{\mathbf{y}_{i,1}, \mathbf{y}_{i,2}, \dots, \mathbf{y}_{i,n_i}\}$ are unknown. Suppose we have a model denoted by $f(\theta)$, a binary MIL classification task is to give bag-level prediction $\hat{\mathbf{Y}}_i = f(\mathbf{X}_i; \theta) \in \{0, 1\}$ as close to the bag-level label $\mathbf{Y}_i \in \{0, 1\}$ as possible, i.e., $\arg \min_{\theta} L(\hat{\mathbf{Y}}_i, \mathbf{Y}_i)$, where L denotes the loss function and n_i is the number of instances of i -st bag-level data. The MIL constraints are illustrated as follows.

$$\mathbf{Y}_i = \begin{cases} x = 0, \text{ iff } \sum \mathbf{y}_{i,j} = 0, & \mathbf{y}_{i,j} \in \{0, 1\}, \\ y = 1, \text{ otherwise} \end{cases} \quad (1)$$

Apply Transformer to MIL-based WSIs Classification

In the context of a Transformer-based binary classification problem on WSIs, we define bag-level data as referring to WSIs, where label 0 denotes normal WSI and label 1 denotes WSI containing tumors. To reduce computational complexity, we can employ an embedding-based approach, where we initially fed segmented patches to a patch encoder extractor (e.g., ResNet(He et al. 2016)) and use the resulting

feature sequences as input to the Transformer. Due to the gigapixel of WSI, the resulting feature sequences are too long to perform MSA. Therefore, we propose a multi-level MIL framework for applying Transformer.

Build Multi-level Bags for WSIs

In this section, we demonstrate how to build hierarchical bags for WSI. The construction process involves two primary stages, aiming at building a higher-level bag from its corresponding lower-level counterpart. The first stage is grouping and masking, where the lower bag is first divided into sub-bags by a grouping operator with a fixed masking ratio. In the second stage, these sub-bags are used to produce higher-level bags by a generator. We instantiated a messenger-based (Fang et al. 2022) generator, where *MSG* tokens are the raw material to produce a higher-level bag.

Grouping Operators The utilization of grouping operators allows us to partition lengthy sequences into shorter sub-bags and introduce prior information to the data, thus enabling performing MSA. We instantiated types of grouping operators. Each of these operators possesses its own set of pros and cons.

- *Coordinate grouping*: we employ the original coordinates of patches as the basis for grouping. Specifically, we preserve the central coordinates of all clipped patches from a WSI when pre-processing, and use these coordinates for K-Means (Hartigan and Wong 1979) clustering. Sub-bags are created by the index of clustering results.
- *Embedding grouping*: we use the cosine distance between embeddings for clustering, then treat the result as sub-bags. This approach does not require additional coordinate information.
- *Random grouping*: we randomly group the embeddings to specific numbers of sub-bags.
- *Sequential grouping*: the embeddings are grouped into numbers of sub-bags in sequential order, with the original patches arranged on the WSI from left to right and top to bottom.
- *MSA grouping*: the embeddings are grouped into numbers of sub-bags according to attention scores produced by multi-head self-attention (MSA). First, we use *Random grouping* to make a fixed number of sub-bags, then perform MSA within each sub-bag to obtain attention scores. Select *top-k* instances within each sub-bag, the selected instances from one original group are regarded as a new group, which is presented as Alg. 1. This enables grouping operators can be supervised.

Coordinate grouping introduces additional information into sub-bags. *Embedding grouping* considers the similarity between patches and does not require an additional step in pre-processing. But these clustering-based grouping methods incur higher computational resource costs. *Random grouping* is simple, and it may bring a benefit for unbalanced data problems. But the randomness of this method sometimes makes the performance unstable when training. *MSA grouping* requires additional computational costs, however, we can supervise grouping by applying specific prior bias.

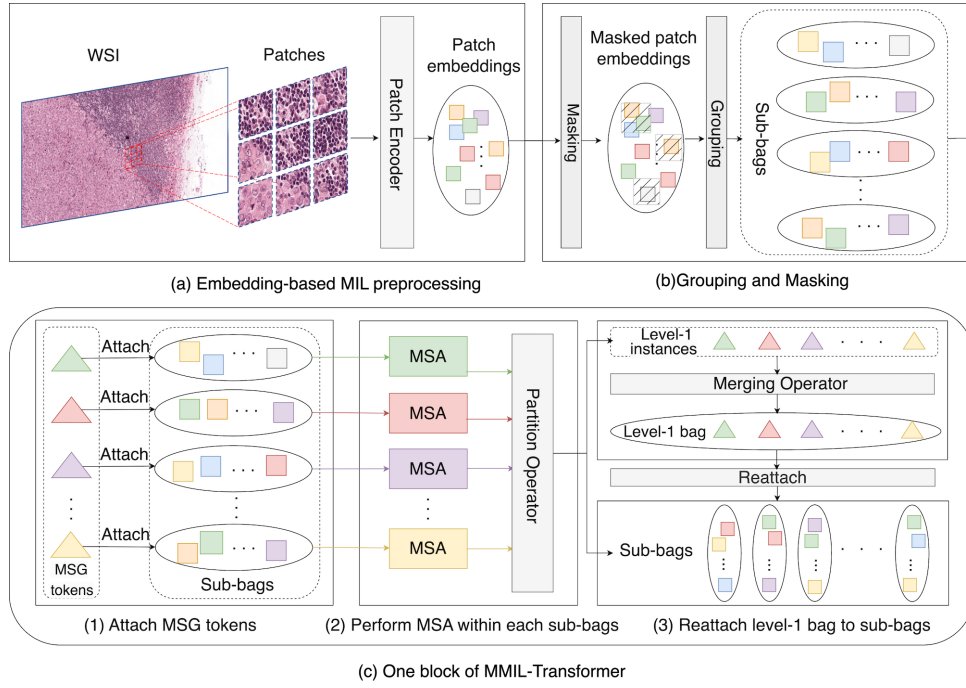


Figure 2: Overview of a two-level MMIL-Transformer. (a) WSI Pre-processing: 1) Background removal; 2) Clip tissue images into patches; 3) Mapping patches to feature embeddings. (b) Grouping and Masking: split feature embeddings into sub-bags and mask fixed ratio of embeddings; (c) One block of MMIL-Transformer: (1) Attach *MSG* tokens to each sub-bag. (2) Perform MSA within each sub-bag then part sub-bags from *MSG* tokens; 3) Merge Parted *MSG* tokens to build a level-1 bag, then reattach all tokens in level-1 bag to level-0 sub-bags;

Algorithm 1: *MSA Grouping*

Input: Bag-level data \mathbf{X}

Output: Sub-bags $\{G_1, G_2, \dots, G_g\}$

- 1: Grouping \mathbf{X}^l to g sub-bags by *Random grouping* r ;
 $\{G_1, G_2, \dots, G_g\} \leftarrow r(\mathbf{X}_h^l)$
 - 2: **while** $j < g$ **do**
 - 3: Perform MSA within each sub-bag G_j to obtain attention scores S_j ;
 $S_j \leftarrow \text{MSA}(G_j)$
 - 4: According to S_j , select *top-k* instances from G_j to build a new group;
 $H_j \leftarrow \text{Top}_k(G_j)$
 - 5: G_j is divided to H_j and L_j , where $G_j = H_j + L_j$;
 $G_j \leftarrow (H_j, L_j)$
 - 6: **end while**
-

Additionally, grouping operators can be designed freely for different requirements.

Embedding-wise masking Corresponding with grouping operators, we further introduce a *masking mechanism* to speed up the model and enhance its performance. Specifically, after partitioning sequences into sub-bags, a fixed ratio of the sub-bags will be masked. These masked sub-bags will be deposited for the following processing.

Build a higher-level instance There are many types of methods that can be used to build higher-level instances. For example, downsampling and pooling. We instantiated one higher-level instance generator by using the messenger mechanism (Fang et al. 2022). As shown in Fig. 2(c), m *MSG* tokens $T_{MSG}^j \in \mathbb{R}^{m \times C}$ will be attached to each sub-bag $G_j \in \mathbb{R}^{w_j \times C}$ as $G_j' \in \mathbb{R}^{(w_j+m) \times C}$, where C denotes the embedding channel of patch feature, w_j denotes the number of members in j -th sub-bag. Therefore, one WSI is divided into *MSG* token attached sub-bags $\{G_1', G_2', \dots, G_g'\}$. MSA is performed within each sub-bag between both feature embeddings and *MSG* tokens. *MSG* tokens can capture information from the corresponding sub-bag with attention. Finally, all *MSG* tokens from different sub-bags are collected as higher-level instances, then undergo a merging operation to produce a higher-level bag. Moreover, a class (*CLS*) token is attached to the higher-level bag for the classification task. Actually, this *CLS* token can be regarded as the final-level bag.

Merging Operation Merging operation aims to collect and merge instances generated from sub-bags for producing a higher-level bag. There are many merge operations, including but not limited to shuffle and average. Corresponding with the *MSG* based generation method, we implement self-attention to merge instances. In this case, after performing MSA with patch embeddings, the patch embeddings are partitioned from the *MSG* tokens, and the *MSG* tokens

Algorithm 2: Bulid k -level bags though MSG tokens

Input: Bag-level data \mathbf{X}_h^0
Output: Set of k level bags \mathbf{X}_h^K

- 1: **while** level $< k$ **do**
- 2: Grouping and masking \mathbf{X}_h^l to g sub-bags by operation c ;
 $\{G_1, G_2, \dots, G_g\} \leftarrow c(\mathbf{X}_h^l)$
- 3: Attach MSG tokens to each sub-bags;
 $G_j' \leftarrow \text{Concat}(T_{MSG}^j; G_j), \quad j \in \{1, 2, \dots, g\};$
- 4: Perform MSA in each sub-bag;
 $G_j' \leftarrow \text{MSA}(G_j') + G_j';$
- 5: Merging all MSG tokens to build higher level bag;
 $\mathbf{X}_h^{l+1} \leftarrow \text{Merge}(T_{MSG}^1, T_{MSG}^2, \dots, T_{MSG}^g)$
- 6: Append \mathbf{X}_h^{l+1} to \mathbf{X}_h^K .
- 7: **end while**
- 8: Attach CLS token to highest level bag;
 $\mathbf{X}_h^k \leftarrow \text{Concat}(\mathbf{X}_h^k, T_{cls})$
- 9: **return** \mathbf{X}_h^K

are subsequently fed into a Transformer to build higher-level bags.

Overall, the process to generate multi-level bags for WSI can be summarized as Alg. 2.

MMIL-Transformer

We now present MMIL-Transformer. As shown in Fig. 2, we first preprocess WSI following the procedure mentioned in Fig. 2(a), which converts high-resolution WSI to patch embeddings. These embeddings are fed into MMIL-Transformer layers. In one basic layer, higher-level bags are generated through Alg. 2. It is worth noting that the higher-level bags are derived from the MSG tokens obtained from lower-level sub-bags. This relationship allows for their reattachment to the corresponding lower-level sub-bags, thereby enabling the implementation of a multi-layer design for MMIL-Transformer. Finally, the model will give a prediction to one WSI by performing MLP to the class token T_{cls} . We summarize the whole MMIL-Transformer as Alg. 3.

Complexity Analysis For a sequence $S \in \mathbb{R}^{p \times C}$, where p is the length of S , C is number of channels. The complexity of the original MSA per layer is $\mathcal{O}(p^2 \times C)$. Assuming we divide S into g sub-bags with a masking ratio of $0 \leq r < 1$, denoted as $G \in \mathbb{R}^{g \times \frac{p}{g} \times (1-r) \times C}$. The complexity of MSA per sub-bag is $\mathcal{O}((\frac{p(1-r)}{g})^2 \times C)$. Thus, for one specific level bag, the total complexity of MSA per layer in MMIL-Transformer is $\mathcal{O}(\frac{1}{g} \times p^2(1-r)^2 \times C)$.

Experiments

To demonstrate the superior performance of the proposed MMIL-Transformer, we conducted various experiments on the CAMELYON16 (Bejnordi et al. 2017) dataset and TCGA-NSCLC (Tomczak, Czerwińska, and Wiznerowicz 2015) dataset.

Algorithm 3: MMIL-Transformer

Input: Bag of instances $\mathbf{X}_i = \{x_{i,1}, x_{i,2}, \dots, x_{i,n}\}$
Output: Bag-level prediction $\hat{\mathbf{Y}}_i$

- 1: Embed the instances to feature space by h ;
 $\mathbf{X}_h \leftarrow h(\mathbf{X}_i)$, where $\mathbf{X}_h \in \mathbb{R}^{n \times C}$;
- 2: **for** each layer **do**
- 3: Build k -level bags \mathbf{X}_h^K by Alg. 2, denoted by MLB;
 $X_h^K = \text{MLB}(X_h)$, where $X_h^K = \{X_h^0, \dots, X_h^k\}$;
- 4: Reattach X_h^{l+1} to X_h^l for all $X_h^l \in X_h^K$;
 $X_h^l = \text{Concat}(X_h^{l+1}, X_h^l)$, for $l \in \{0, 1, \dots, k\}$;
- 5: Fed X_h^0 to next layer;
- 6: **end for**
- 7: Give prediction $\hat{\mathbf{Y}}$ though T_{cls} ;
 $\hat{\mathbf{Y}} \leftarrow \text{MLP}(T_{cls})$
- 8: **return** $\hat{\mathbf{Y}}$

Dataset and Evaluation Metrics CAMELYON16 is a public dataset for metastasis detection in hematoxylin and eosin (H&E) stained WSIs of lymph node sections. The dataset contains 270 training WSIs and 129 test WSIs. We perform pre-processing at $\times 20$ magnification, which produces 4.6 million 256×256 non-overlapping patches. All patches are mapped to feature embeddings by ImageNet pre-trained ResNet50 (He et al. 2016) baseline.

The TCGA-NSCLC dataset focuses on non-small cell lung cancer (NSCLC), encompassing two types of carcinoma: Lung Squamous Cell Carcinoma (TGCA-LUSC) and Lung Adenocarcinoma (TCGA-LUAD). TCGA-NSCLC comprises a total of 1053 diagnostic WSIs, with 541 slides from 478 cases for LUAD and 512 slides from 478 cases for LUSC. For pre-processing, we adopt the same configuration as DSMIL (Li, Li, and Eliceiri 2021), where a total of 1046 WSIs are involved in the computation. We split the dataset in the ratio of training:validation:test = 60:15:25, resulting in 627 training WSIs, 156 validation WSIs and 263 test WSIs.

To evaluate the classification performance, we utilized accuracy and area under the curve (AUC) scores as the evaluation metrics. In all experiments, the accuracy was calculated using a fixed threshold of 0.5.

Experiments Details We employ cross-entropy as our loss function, and the Adma optimizer was employed with a learning rate of $1e-4$ and weight decay of $1e-5$. The default number of basic layers is 2. For the CAMELYON16 dataset, we grouped the embeddings into 10 sub-bags using the *random grouping* operator and randomly masked the sub-bags by a ratio of 0.6. As for the TCGA-NSCLC dataset, we employed *random grouping* to split the embeddings into 4 sub-bags. In both datasets, one single MSG token is attached to each sub-bag. These MSG tokens are then used to construct higher-level bags structure for later modules. All experiments were conducted using a 24GB RTX 3090 GPU.

Results on WSI Classification

The binary classification tasks encompass the identification of positive and negative cases within the CAMELYON16

Table 1: Results on CAMELYON16 and TCGA-NSCLC using ResNet-50 as the patch encoder

Method	Publication	CAMELYON16		TCGA-NSCLC	
		Accuracy	AUC	Accuracy	AUC
ABMIL (Ilse, Tomczak, and Welling 2018)	ICML 2018	0.8682	0.8760	0.7719	0.8656
PT-MTA (Li et al. 2019)	MICCAI 2019	0.8217	0.8454	0.7379	0.8299
MIL-RNN (Campanella et al. 2019)	Nature Med 2019	0.8450	0.8880	0.8619	0.9107
DSMIL (Li, Li, and Eliceiri 2021)	CVPR 2021	0.7985	0.8179	0.8058	0.8925
CLAM-SB (Lu et al. 2021)	Nature BME 2021	0.8760	0.8809	0.8180	0.8818
CLAM-MB (Lu et al. 2021)	Nature BME 2021	0.8372	0.8679	0.8422	0.9377
TransMIL (Shao et al. 2021)	NeurIPS 2021	0.8837	0.9309	0.8835	0.9603
DGMIL (Qu et al. 2022)	MICCAI 2022	0.8018	0.8368	0.9200	0.9702
DTFD-MIL (AFS) (Zhang et al. 2022)	CVPR 2022	0.908	0.946	0.891	0.951
DTFD-MIL (MaxS) (Zhang et al. 2022)	CVPR 2022	0.899	0.941	0.894	0.961
MSG-Transformer (Fang et al. 2022)	CVPR 2022	0.8062	0.8313	0.9354	0.9874
MMIL-Transformer	-	0.9341	0.9474	0.9437	0.9904

dataset, LUSC and LUAD subtypes within the TCGA-NSCLC dataset. All results are presented in Tab. 1. Notably, except MMIL-Transformer(CTransPath) uses CTransPath as the patch encoder, all others use ResNet50. Compared with other state-of-the-art methods (Shao et al. 2021; Lu et al. 2021; Li, Li, and Eliceiri 2021; Campanella et al. 2019; Ilse, Tomczak, and Welling 2018; Li et al. 2019; Zhang et al. 2022; Qu et al. 2022), the proposed MMIL-Transformer consistently achieves superior results in both accuracy and AUC score on both datasets. Note that all test experiments are conducted 10 times in test datasets to calculate the average accuracy and AUC.

The CAMELYON16 dataset exhibits an imbalanced distribution of normal tissue patches and tumor tissue patches, posing significant challenges for the classification task. However, MMIL-Transformer overcomes these challenges and achieves a notable improvement of 3.51% accuracy compared to DTFD-MIL(MaxMinS). Compared to the approximate attention method TransMIL, MMIL-Transformer achieves an improvement of 5.04% accuracy and 1.65% AUC. CLAM, PT-MTA, and ABMIL do not consider the correlation between instances, which leads to limited performance. In comparison to other non-attention methods, the utilization of clustering operation in CLAM has enabled it to achieve relatively better performance. While MSG-Transformer adeptly employs the *MSG* for local information exchange, its performance remains constrained in the absence of accurate local-to-global self-attention.

In the TCGA-NSCLC dataset, there is a higher abundance of positive tissue patches compared to negatives, resulting in relatively easier identification of LUSC with LUAD. All mentioned methods achieve relatively better performance than their performance on CAMELYON16. However, MMIL-Transformer stands out with an impressive accuracy of 94.37% and AUC score of 99.04%.

We also compare MMIL-Transformer with other methods by using CTransPath (Wang et al. 2022) as the patch encoder. The results are shown in Tab. 2. In this part, we use the same dataset configurations as (Lin et al. 2023). We use *MSA grouping* with a masking ratio of 0.2 to make 10 sub-bags for MMIL-Transformer on CAMELYON16, *MSA grouping* without masking to make 4 sub-bags on TCGA-NSCLC. Compared with the most recent

works like IBMIL((Lin et al. 2023)), our methods demonstrate competitive performances. Compared with IBMIL-TransMIL, MMIL-Transformer achieves 97.67%(+1.55%) on the CAMELYON16 and 94.28%(+0.47%) on the TCGA-NSCLC. However, MMIL-Transformer is slightly lower than IBMIL-TransMIL on the AUC, with a mere -0.2% on the CAMELYON16.

Table 2: Results on CAMELYON16 and TCGA-NSCLC using CTransPath as the patch encoder

Dataset	Method	Accuracy	AUC
CAMELYON16	TransMIL (NeurIPS 2021)	0.9457	0.9588
	DTFD-MIL (CVPR 2022)	0.9535	0.9618
	IBMIL-TransMIL (CVPR 2023)	0.9612	0.9700
	MMIL-Transformer	0.9767	0.9680
TCGA-NSCLC	ABMIL (ICML2018)	0.9048	0.9587
	IBMIL-DSMIL (CVPR 2023)	0.9143	0.9751
	IBMIL-TransMIL (CVPR 2023)	0.9381	0.9724
	MMIL-Transformer	0.9428	0.9788

Ablation Study

We further conducted a series of ablation studies using ResNet-50 as the patch encoder to determine the contribution of several proposed modules.

Effects of Grouping Operator To determine the impact of different grouping operators, we performed a series of experiments while keeping the other configurations unchanged. Notably, to avoid the effects of randomness, we employ *coordinate grouping* instead of *random grouping* on CAMELYON16, *embedding grouping* instead of *random grouping* on TCGA-NSCLC. The masking ratio is 0 for this part.

We first study the influence of the number of sub-bags. The results are shown in Tab. 3. In CAMELYON16 the test AUC decays as the number of sub-bags increases. This behavior can be attributed to the trade-off between the number of sub-bags and available memory resources. Larger numbers of sub-bags require less memory and computational cost, but it makes obstacles to effective communication between them. It can be predicted that the accuracy will be lower as the number of sub-bags increases. In TCGA-NSCLC, there are relatively fewer patches (with a minimum

of 23 patches) in WSIs, we were able to split the dataset into up to 6 sub-bags using clustering. Compared with CAMELYON16, the performance deterioration in TCGA-NSCLC is relatively minor.

Table 3: Effects of Different Grouping Numbers.

Dataset	Sub-bags number	Accuracy	AUC
CAMELYON16	10	0.8992	0.9500
	16	0.8682	0.9305
	32	0.8992	0.9314
	2	0.9354	0.9896
TCGA-NSCLC	4	0.9392	0.9887
	6	0.9316	0.9890

We also studied the effect of different grouping methods, the experiment was conducted on CAMELYON16, and the results are shown in Tab. 4. An interesting observation is that the incorporation of additional coordinate information leads to a performance decline in terms of accuracy when compared to *random grouping*. In our view, using random grouping alleviates the influence of instance imbalance. Through the process of *random grouping*, each sub-bag has the potential to be allocated positive instances. This enables the attention mechanism to focus on the positive instances within each sub-bag, thereby enhancing the accuracy of the model. Conversely, the incorporation of positional information may give rise to a substantial quantity of sub-bags that lack positive instances, thereby exacerbating the issue of imbalance on higher-level bags. On the other hand, embedding grouping, which does not need additional information, yields relatively lower accuracy and AUC scores. When we group the embeddings in sequential order, thereby utilizing ill spatial information, the resulting scores in accuracy and AUC are lower. *MSA grouping* achieves the highest accuracy but requires more computational resources.

Table 4: Effects of Different Grouping Methods

Dataset	Method	Accuracy	AUC
CAMELYON16	Coordinate grouping	0.8992	0.9500
	Embedding grouping	0.8682	0.9216
	Sequential grouping	0.8604	0.9097
	Random grouping	0.9178	0.9219
	MSA grouping	0.9224	0.9363

Effects of Masking We conducted several experiments to determine the effects of the masking mechanism. The grouping method is *random grouping* on the dataset. The results are presented in Tab.5. Including the masking mechanism results in a 1.63% accuracy enhancement in the case of 10 sub-bags number. As the number of sub-bags goes up, accuracy decrease without masking. However, the masking mechanism recoups the performance decline.

Effects of Multi-level Framework In CAMELYON16, patches of different WSIs in $\times 20$ magnification range from 142 to 55852. In TCGA-NSCLC, patches range from 23

Table 5: Effects of Different Masking Ratio On CAMELYON16

Sub-bags number	Masking ratio	Accuracy	AUC
10	0.6	0.9341	0.9474
	0.3	0.9302	0.9372
	0	0.9178	0.9219
16	0.6	0.9302	0.9395
	0.3	0.9147	0.9373
	0	0.8682	0.9305
32	0.6	0.9302	0.9263
	0.3	0.9069	0.9222
	0	0.8992	0.9314

to 14990. The minimum number of patches determines the maximum number of sub-bags that can be formed, consequently limiting the dimension of higher-level bags. Ablation experiments are conducted on CAMELYON16 by using *coordinate grouping* for the reason of its relative more patches. Again, due to the impracticality of directly performing MSA on level-0 bags as the sequences are too long, we conduct this part experiments by using a Nyström Attention method for fairness. The results are shown in Tab. 6. MMIL-Transformer achieves a similar result as TransMIL in 0-level bags due to they both employ approximate attention. The performance on level-1 is much worse than level-0 due to the trade-off mentioned before and the information loss from approximate-attention. The crucial aspect is that this multi-level framework enables the suggested model to perform non-approximate MSA, leading to significantly enhanced performance.

Table 6: Effects of Multi-level Framework.

Dataset	k	Accuracy	AUC	Approximate-attention
CAMELYON16	0	0.8759	0.9227	✓
	1	0.6667	0.6650	✓
	1	0.8992	0.9500	×

Discussion and Conclusion

In our work, we proposed MMIL, a multi-level MIL learning strategy. Based on this strategy, we construct a MMIL-Transformer model for long-sequence MIL tasks. The proposed model first splits bag-level data into sub-bags, then builds hierarchical bags from those sub-bags for the following stages. This enables MMIL-Transformer to apply non-approximate MSA, which significantly enhances its performance. Moreover, the masking mechanism equivalently enhances the data while also further reducing the computational complexity. Overall, MMIL is an effective MIL learning strategy, by which MMIL-Transformer can better establish local-global connections with less complexity. This makes it more suitable for large-scale unbalanced/balanced MIL learning.

Limitations and Future Work When dealing with CAMELYON16, we find the performance is more sensitive

to the grouping results due to the unbalanced problem. There should be a more suitable grouping operator for making the performance more stable. We will explore these issues in the follow-up work.

References

- Bankhead, P.; Loughrey, M. B.; Fernández, J. A.; Dombrowski, Y.; McArt, D. G.; Dunne, P. D.; McQuaid, S.; Gray, R. T.; Murray, L. J.; Coleman, H. G.; et al. 2017. QuPath: Open source software for digital pathology image analysis. *Scientific reports*, 7(1): 1–7.
- Bejnordi, B. E.; Veta, M.; Van Diest, P. J.; Van Ginneken, B.; Karssemeijer, N.; Litjens, G.; Van Der Laak, J. A.; Hermesen, M.; Manson, Q. F.; Balkenhol, M.; et al. 2017. Diagnostic assessment of deep learning algorithms for detection of lymph node metastases in women with breast cancer. *Jama*, 318(22): 2199–2210.
- Beltagy, I.; Peters, M. E.; and Cohan, A. 2020. Longformer: The long-document transformer. *arXiv preprint arXiv:2004.05150*.
- Campanella, G.; Hanna, M. G.; Geneslaw, L.; Miralflor, A.; Werneck Krauss Silva, V.; Busam, K. J.; Brogi, E.; Reuter, V. E.; Klimstra, D. S.; and Fuchs, T. J. 2019. Clinical-grade computational pathology using weakly supervised deep learning on whole slide images. *Nature medicine*, 25(8): 1301–1309.
- Chen, J.; Lu, Y.; Yu, Q.; Luo, X.; Adeli, E.; Wang, Y.; Lu, L.; Yuille, A. L.; and Zhou, Y. 2021. Transunet: Transformers make strong encoders for medical image segmentation. *arXiv preprint arXiv:2102.04306*.
- Chikontwe, P.; Kim, M.; Nam, S. J.; Go, H.; and Park, S. H. 2020. Multiple instance learning with center embeddings for histopathology classification. In *Medical Image Computing and Computer Assisted Intervention–MICCAI 2020: 23rd International Conference, Lima, Peru, October 4–8, 2020, Proceedings, Part V 23*, 519–528. Springer.
- Child, R.; Gray, S.; Radford, A.; and Sutskever, I. 2019. Generating long sequences with sparse transformers. *arXiv preprint arXiv:1904.10509*.
- Dietterich, T. G.; Lathrop, R. H.; and Lozano-Pérez, T. 1997. Solving the multiple instance problem with axis-parallel rectangles. *Artificial intelligence*, 89(1-2): 31–71.
- Fang, J.; Xie, L.; Wang, X.; Zhang, X.; Liu, W.; and Tian, Q. 2022. Msg-transformer: Exchanging local spatial information by manipulating messenger tokens. In *Proceedings of the IEEE/CVF Conference on Computer Vision and Pattern Recognition*, 12063–12072.
- Goode, A.; Gilbert, B.; Harkes, J.; Jukic, D.; and Satyanarayanan, M. 2013. OpenSlide: A vendor-neutral software foundation for digital pathology. *Journal of pathology informatics*, 4(1): 27.
- Hartigan, J. A.; and Wong, M. A. 1979. Algorithm AS 136: A k-means clustering algorithm. *Journal of the royal statistical society. series c (applied statistics)*, 28(1): 100–108.
- Hashimoto, N.; Fukushima, D.; Koga, R.; Takagi, Y.; Ko, K.; Kohno, K.; Nakaguro, M.; Nakamura, S.; Hontani, H.; and Takeuchi, I. 2020. Multi-scale domain-adversarial multiple-instance CNN for cancer subtype classification with unannotated histopathological images. In *Proceedings of the IEEE/CVF conference on computer vision and pattern recognition*, 3852–3861.
- He, K.; Zhang, X.; Ren, S.; and Sun, J. 2016. Deep residual learning for image recognition. In *Proceedings of the IEEE conference on computer vision and pattern recognition*, 770–778.
- He, L.; Long, L. R.; Antani, S.; and Thoma, G. R. 2012. Histology image analysis for carcinoma detection and grading. *Computer methods and programs in biomedicine*, 107(3): 538–556.
- Hu, H.; Zhang, Z.; Xie, Z.; and Lin, S. 2019. Local relation networks for image recognition. In *Proceedings of the IEEE/CVF International Conference on Computer Vision*, 3464–3473.
- Huang, Z.; Wang, X.; Huang, L.; Huang, C.; Wei, Y.; and Liu, W. 2019. Ccnet: Criss-cross attention for semantic segmentation. In *Proceedings of the IEEE/CVF international conference on computer vision*, 603–612.
- Ilse, M.; Tomczak, J.; and Welling, M. 2018. Attention-based deep multiple instance learning. In *International conference on machine learning*, 2127–2136. PMLR.
- Jaderberg, M.; Simonyan, K.; Zisserman, A.; et al. 2015. Spatial transformer networks. *Advances in neural information processing systems*, 28.
- Kanavati, F.; Toyokawa, G.; Momosaki, S.; Rambeau, M.; Kozuma, Y.; Shoji, F.; Yamazaki, K.; Takeo, S.; Iizuka, O.; and Tsuneki, M. 2020. Weakly-supervised learning for lung carcinoma classification using deep learning. *Scientific reports*, 10(1): 9297.
- Keeler, J.; Rumelhart, D.; and Leow, W. 1990. Integrated segmentation and recognition of hand-printed numerals. *Advances in neural information processing systems*, 3.
- Kitaev, N.; Kaiser, Ł.; and Levskaya, A. 2020. Reformer: The efficient transformer. *arXiv preprint arXiv:2001.04451*.
- Lerousseau, M.; Vakalopoulou, M.; Classe, M.; Adam, J.; Battistella, E.; Carré, A.; Estienne, T.; Henry, T.; Deutsch, E.; and Paragios, N. 2020. Weakly supervised multiple instance learning histopathological tumor segmentation. In *Medical Image Computing and Computer Assisted Intervention–MICCAI 2020: 23rd International Conference, Lima, Peru, October 4–8, 2020, Proceedings, Part V 23*, 470–479. Springer.
- Li, B.; Li, Y.; and Elieceiri, K. W. 2021. Dual-stream multiple instance learning network for whole slide image classification with self-supervised contrastive learning. In *Proceedings of the IEEE/CVF conference on computer vision and pattern recognition*, 14318–14328.
- Li, W.; Nguyen, V.-D.; Liao, H.; Wilder, M.; Cheng, K.; and Luo, J. 2019. Patch transformer for multi-tagging whole slide histopathology images. In *Medical Image Computing and Computer Assisted Intervention–MICCAI 2019: 22nd International Conference, Shenzhen, China, October 13–17, 2019, Proceedings, Part I 22*, 532–540. Springer.

- Lin, T.; Yu, Z.; Hu, H.; Xu, Y.; and Chen, C.-W. 2023. Interventional bag multi-instance learning on whole-slide pathological images. In *Proceedings of the IEEE/CVF Conference on Computer Vision and Pattern Recognition*, 19830–19839.
- Liu, Z.; Lin, Y.; Cao, Y.; Hu, H.; Wei, Y.; Zhang, Z.; Lin, S.; and Guo, B. 2021. Swin transformer: Hierarchical vision transformer using shifted windows. In *Proceedings of the IEEE/CVF international conference on computer vision*, 10012–10022.
- Lu, M. Y.; Williamson, D. F.; Chen, T. Y.; Chen, R. J.; Barbieri, M.; and Mahmood, F. 2021. Data-efficient and weakly supervised computational pathology on whole-slide images. *Nature biomedical engineering*, 5(6): 555–570.
- Naik, N.; Madani, A.; Esteva, A.; Keskar, N. S.; Press, M. F.; Ruderman, D.; Agus, D. B.; and Socher, R. 2020. Deep learning-enabled breast cancer hormonal receptor status determination from base-level H&E stains. *Nature communications*, 11(1): 5727.
- Qu, L.; Luo, X.; Liu, S.; Wang, M.; and Song, Z. 2022. Dgmil: Distribution guided multiple instance learning for whole slide image classification. In *International Conference on Medical Image Computing and Computer-Assisted Intervention*, 24–34. Springer.
- Ramachandran, P.; Parmar, N.; Vaswani, A.; Bello, I.; Levskaya, A.; and Shlens, J. 2020. Stand-alone self-attention in vision models. *Advances in neural information processing systems*, 32.
- Shao, Z.; Bian, H.; Chen, Y.; Wang, Y.; Zhang, J.; Ji, X.; et al. 2021. Transmil: Transformer based correlated multiple instance learning for whole slide image classification. *Advances in neural information processing systems*, 34: 2136–2147.
- Srinidhi, C. L.; Ciga, O.; and Martel, A. L. 2021. Deep neural network models for computational histopathology: A survey. *Medical Image Analysis*, 67: 101813.
- Tan, M.; and Le, Q. 2019. Efficientnet: Rethinking model scaling for convolutional neural networks. In *International conference on machine learning*, 6105–6114. PMLR.
- Tian, Y.; Yang, L.; Wang, W.; Zhang, J.; Tang, Q.; Ji, M.; Yu, Y.; Li, Y.; Yang, H.; and Qian, A. 2019. Computer-aided detection of squamous carcinoma of the cervix in whole slide images. *arXiv preprint arXiv:1905.10959*.
- Tomczak, K.; Czerwińska, P.; and Wiznerowicz, M. 2015. Review The Cancer Genome Atlas (TCGA): an immeasurable source of knowledge. *Contemporary Oncology/Współczesna Onkologia*, 2015(1): 68–77.
- Tomita, N.; Abdollahi, B.; Wei, J.; Ren, B.; Suriawinata, A.; and Hassanpour, S. 2019. Attention-based deep neural networks for detection of cancerous and precancerous esophagus tissue on histopathological slides. *JAMA network open*, 2(11): e1914645–e1914645.
- Vaswani, A.; Shazeer, N.; Parmar, N.; Uszkoreit, J.; Jones, L.; Gomez, A. N.; Kaiser, Ł.; and Polosukhin, I. 2017. Attention is all you need. *Advances in neural information processing systems*, 30.
- Wang, S.; Li, B. Z.; Khabsa, M.; Fang, H.; and Ma, H. 2020. Linformer: Self-attention with linear complexity. *arXiv preprint arXiv:2006.04768*.
- Wang, X.; Girshick, R.; Gupta, A.; and He, K. 2018a. Non-local neural networks. In *Proceedings of the IEEE conference on computer vision and pattern recognition*, 7794–7803.
- Wang, X.; Yan, Y.; Tang, P.; Bai, X.; and Liu, W. 2018b. Revisiting multiple instance neural networks. *Pattern Recognition*, 74: 15–24.
- Wang, X.; Yang, S.; Zhang, J.; Wang, M.; Zhang, J.; Yang, W.; Huang, J.; and Han, X. 2022. Transformer-based unsupervised contrastive learning for histopathological image classification. *Medical image analysis*, 81: 102559.
- Xiong, Y.; Zeng, Z.; Chakraborty, R.; Tan, M.; Fung, G.; Li, Y.; and Singh, V. 2021. Nyströmformer: A nyström-based algorithm for approximating self-attention. In *Proceedings of the AAAI Conference on Artificial Intelligence*, volume 35, 14138–14148.
- Xu, G.; Song, Z.; Sun, Z.; Ku, C.; Yang, Z.; Liu, C.; Wang, S.; Ma, J.; and Xu, W. 2019. Camel: A weakly supervised learning framework for histopathology image segmentation. In *Proceedings of the IEEE/CVF International Conference on computer vision*, 10682–10691.
- Zaheer, M.; Guruganesh, G.; Dubey, K. A.; Ainslie, J.; Alberti, C.; Ontanon, S.; Pham, P.; Ravula, A.; Wang, Q.; Yang, L.; et al. 2020. Big bird: Transformers for longer sequences. *Advances in neural information processing systems*, 33: 17283–17297.
- Zhang, H.; Meng, Y.; Zhao, Y.; Qiao, Y.; Yang, X.; Coupland, S. E.; and Zheng, Y. 2022. DTFD-MIL: Double-tier feature distillation multiple instance learning for histopathology whole slide image classification. In *Proceedings of the IEEE/CVF Conference on Computer Vision and Pattern Recognition*, 18802–18812.
- Zhao, H.; Jia, J.; and Koltun, V. 2020. Exploring self-attention for image recognition. In *Proceedings of the IEEE/CVF conference on computer vision and pattern recognition*, 10076–10085.
- Zhou, Z.-H. 2018. A brief introduction to weakly supervised learning. *National science review*, 5(1): 44–53.